Nano Materials Science xxx (xxxx) xxx

Contents lists available at ScienceDirect

Nano Materials Science

journal homepage: www.keaipublishing.com/cn/journals/nano-materials-science/

Alkali metal cations change the hydrogen evolution reaction mechanisms at Pt electrodes in alkaline media

Yamen Taji [a], Alexandra Zagalskaya [b], Iman Evazzade [b], Sebastian Watzele [a], Kun-Ting Song [a], Song Xue [a,c], Christian Schott [a], Batyr Garlyyev [a], Vitaly Alexandrov [b,*], Elena Gubanova [a,**], Aliaksandr S. Bandarenka [a,d,***]

[a] Physics of Energy Conversion and Storage, Department of Physics, Technical University of Munich, James-Franck-Str. 1, 85748, Garching bei München, Germany
[b] Department of Chemical and Biomolecular Engineering and Nebraska Center for Materials and Nanoscience, University of Nebraska-Lincoln, Lincoln, NE, 68588, United States
[c] Qingdao Key Laboratory of Functional Membrane Material and Membrane Technology, Qingdao Institute of Bioenergy and Bioprocess Technology, Chinese Academy of Sciences, 266101, Qingdao, China
[d] Catalysis Research Center, Technical University of Munich, Ernst-Otto-Fischer-Straße 1, 85748, Garching bei München, Germany

ARTICLE INFO

Keywords:
Hydrogen evolution reaction
Electrolyte effect
Reaction mechanism
Electrocatalysis
Platinum
Density functional theory calculations

ABSTRACT

The effects of seemingly inert alkali metal (AM) cations on the electrocatalytic activity of electrode materials towards reactions essential for energy provision have become the emphasis of substantial research efforts in recent years. The hydrogen and oxygen evolution reactions during alkaline water electrolysis and the oxygen electro-reduction taking place in fuel cells are of particular importance. There is no universal theory explaining all the details of the AM cation effect in electrocatalysis. For example, it remains unclear how "spectator" AM-cations can change the kinetics of electrocatalytic reactions often more significantly than the modifications of the electrode structure and composition. This situation originates partly from a lack of systematic experimental and theoretical studies of this phenomenon. The present work exploits impedance spectroscopy to investigate the influence of the AM cations on the mechanism of the hydrogen evolution reaction at Pt microelectrodes. The activity follows the trend: $Li^+ \geq Na^+ > K^+ > Cs^+$, where the highest activity corresponds to 0.1 M LiOH electrolytes at low overpotentials. We demonstrate that the nature of the AM cations also changes the relative contribution of the Volmer–Heyrovsky and Volmer–Tafel mechanisms to the overall reaction, with the former being more important for LiOH electrolytes. Our density functional theory-based thermodynamics and molecular dynamics calculations support these findings.

1. Introduction

The hydrogen evolution reaction (HER) is a key process for sustainable provision of renewable energy. In alkaline media, it proceeds according to well-accepted mechanisms [1] involving the initial formation of *H adsorbed intermediates (Volmer step, * designates the adsorbed species)

$$H_2O + e^- + M \rightleftharpoons M\text{–}^*H + OH^- \quad (1)$$

followed by either the Heyrovsky step

$$H_2O + M\text{–}^*H + e^- \rightleftharpoons M + H_2 + OH^- \quad (2)$$

or the Tafel step that does not involve the interfacial charge transfer:

$$2^*H \rightleftharpoons H_2 \quad (3)$$

Alkali metal (AM) cations drastically influence the critical parameters at the electrified solid/liquid interfaces, such as the activity [2–7] or the electric double layer capacitance [8–10]. Our recent study on the HER activity of Pt, Ir, Au, and Ag electrodes in different alkaline media shows that weakly hydrated AM cations such as Cs^+ favor the reaction activity of Au and Ag but are detrimental to that of Pt and Ir [11]. Considerable efforts have been devoted to determining the underlying mechanisms of

* Corresponding author.
** Corresponding author.
*** Corresponding author. Catalysis Research Center, Technical University of Munich, Ernst-Otto-Fischer-Straße 1, 85748, Garching bei München, Germany.
E-mail addresses: valexandrov2@unl.edu (V. Alexandrov), elena.gubanova@tum.de (E. Gubanova), bandarenka@ph.tum.de (A.S. Bandarenka).

https://doi.org/10.1016/j.nanoms.2022.09.003

Available online xxxx

this AM cation effect. According to the typical HER volcano plot, hydrogen binding energy modified due to the presence of AM cations has been proposed [11,12]. However, for alkaline HER, water dissociation is recognized as the rate-determining step (RDS) correlating with the hydroxide binding energy [13,14]. Liu et al. [15] suggested that the strongly hydrated AM cations such as Li^+ boost the driving force for OH desorption on Pt electrodes, thus leading to the observed HER activity trend. More recently, our group found that the near-surface concentration of AM cations is up to 80 times higher than bulk concentration, leading to a significant AM cation effect [8,9]. It was shown that the presence of metal cations in increased concentrations at the interface drastically influences the electrocatalysis of oxygen reduction [16,17] and hydrogen evolution [11,18,19] reactions on various electrode surfaces.

Changes to the pH in acidic media affect the mechanism of the HER at Pt electrodes [20]. Several reports also show that at higher pHs the kinetics of the HER is remarkably slower than in the case of acidic media. There are a few hypotheses about the mechanism of such a strong influence. For instance, it was proposed that the solvated AM cations tune the strength of the interaction between the surface-adsorbed *OH species and the Pt electrode surface, affecting activity as a function of the nature of the AM cation [16,17]. Goyal et al. [18] demonstrated that the electrolyte pH and AM cation concentration also impact the HER kinetics at gold electrodes. Besides, Chung et al. reported that the cation can block active sites and alter the structure of near-surface water, or adsorbed hydroxide species may be involved in the hydrogen oxidation/evolution reaction mechanism [21]. It has been proven that raising the cation concentration enhances HER activity significantly at a moderately alkaline pH. However, only a few studies systematically investigate how such metal cations change the mechanism of the reaction of interest. For example, Durst et al. studied the HER mechanism in acidic and alkaline electrolytes on Pt-group metal electrodes and determined that the Volmer reaction was the RDS in both cases [22].

We used Pt-microelectrodes and electrochemical impedance spectroscopy (EIS) in this work to elucidate the influence of the nature of the AM cations on the Volmer–Heyrovsky (VH) or Volmer–Tafel (VT) mechanisms. As shown previously [20], the use of the microelectrodes minimizes typical measurement artifacts such as H_2 bubble formation and enables low-noise EIS measurements at high current densities allowing detailed analysis of reaction mechanisms. It is demonstrated that the AM cations not only influence the HER kinetics at pH = 13 but also change the relative contribution of the VH and VT mechanisms to the overall current.

2. Experimental section

All glassware and Teflon cell parts were cleaned in a piranha solution, a 1:2 mixture of 30% H_2O_2 (Suprapur®, Merck, Germany) and 96% H_2SO_4 (Suprapur®, Merck, Germany), and treated/washed with boiling ultrapure Milli-Q® water with a resistivity of 18.2 MΩ cm before the experiments. Experiments were performed in a double-walled electrochemical cell [23]. A $Hg/HgSO_4$ electrode (SI Analytics, Germany) and a Pt wire/mesh (99.95%, MaTeck, Germany) were used as the reference (RE) and counter electrodes (CE), respectively. Polycrystalline Pt microelectrodes (Ch. Instruments, USA) with a diameter of 25 μm were used as working electrodes in all impedance experiments. All of the potentials in this work are referenced to the reversible hydrogen electrode (RHE) scale. Ar-saturated (Ar 5.0, Air Liquide, Germany) and H_2-saturated (H_2 5.0, Air Liquide, Germany) 0.1 M LiOH (99.998%, Trace Select, Sigma Aldrich), 0.1 M NaOH (99.99%, Semiconductor Grade, Sigma Aldrich), 0.1 M KOH (99.99%, Trace Metal Basis, Sigma Aldrich), and 0.1 M CsOH (99.9%, 50 wt-% Solution, Sigma Aldrich) electrolytes were freshly prepared using ultrapure water. The microelectrodes were electrochemically cleaned by potential cycling in Ar-saturated 0.1 M $HClO_4$ (extra pure, Acros Organics, Belgium) solutions at a scan rate of 50 mV s^{-1} until stable characteristic voltammograms were obtained. The

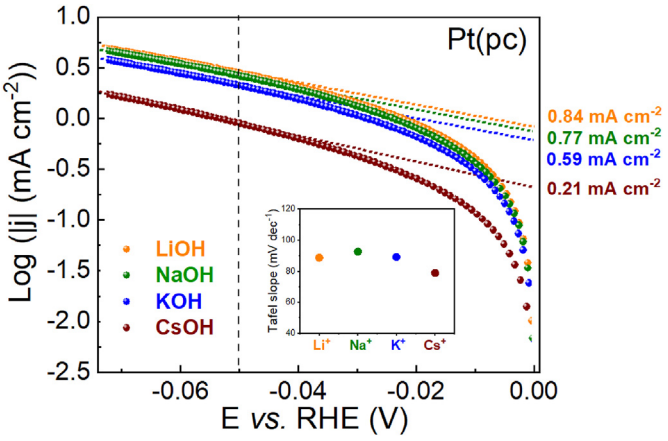

Fig. 1. Activity trend of the HER for Pt(pc) electrodes in 0.1 M AMOH electrolytes (AM = Li^+, Na^+, K^+, Cs^+). The inserted figure provides information about the Tafel slopes for the different electrolytes.

activity data were collected using a 5 mm Pt-polycrystalline disc electrode (Mateck, Germany) at a hanging meniscus configuration using a scan rate of 10 mV s^{-1} in a Pine RDE 710 (USA) rotator with a rotating speed of 1600 rpm.

A VSP-300 (Bio-Logic, France) potentiostat was used in all experiments. EIS spectra were recorded within the potential range between 0.0 V and −0.05 V probing frequencies between 100 kHz and 0.1 Hz (10 mV amplitude). A shunt capacitor was connected between the reference and a dummy electrode to suppress possible potentiostat- and reference electrode-related artifacts. The dummy electrode was placed close to the Luggin capillary. For the EIS data analysis, the "EIS Spectrum Analyzer 1.3″ software was used [24,25]. The quality of the recorded spectra was checked by a Kramers–Kronig relation.

Density Functional Theory (DFT) calculations were carried out utilizing the revised Perdew-Burke-Ernzerhof (revPBE) exchange-correlation functional [26,27] within the Vienna Ab Initio Simulation Package (VASP) [28,29]. The projector-augmented wave (PAW) potentials from the VASP library were employed (Pt, O, H, Li_sv, Na_sv, K_sv, Cs_sv). The D3 approach using the Grimme formalism [30,31] was employed to account for van der Waals interactions. Dipole corrections were included in all surface calculations in the surface normal direction using the VASP tags LDIPOL = TRUE and IDIPOL = 3. All DFT calculations were performed with a cutoff energy of 400 eV, and the convergence criteria for total energies and atomic forces were set to 10^{-4} eV and 0.02 eV $Å^{-1}$, respectively.

The Pt(111) surface was modeled using a periodic slab model with three layers of the Pt metal, with lateral dimensions of 16.64 × 19.22 $Å^2$ and at least 15 Å of the vacuum region. Atomic structures were prepared using the VESTA software [32]. Similar slab models with smaller surface cells were recently employed to simulate the HER and OER over Pt(111) without alkali metal cations [33,34]. Owing to the large cell dimensions, all slab calculations were performed at the Γ point. In this study, we considered both bare and solvated cations; both sets of calculations led to the same conclusions. To find the cation complexes with the first aqueous shell, we ran a series of ab initio molecular dynamics (AIMD) simulations for a slab model with a twice smaller surface cell in which the vacuum region was fully filled with explicit water molecules. At least 6 ps AIMD trajectory was generated for each cation system at room temperature. The atomic configurations of cations with their first water shell were then extracted from the AIMD trajectories for subsequent static DFT optimizations. The inner and outer-sphere complexes were tested, and the latter appeared to be unstable during structural DFT optimization for all cations. This is in agreement with previous DFT studies showing that cations can be specifically adsorbed on metal surfaces [35,36].

The computational hydrogen electrode (CHE) approach [37,38] was

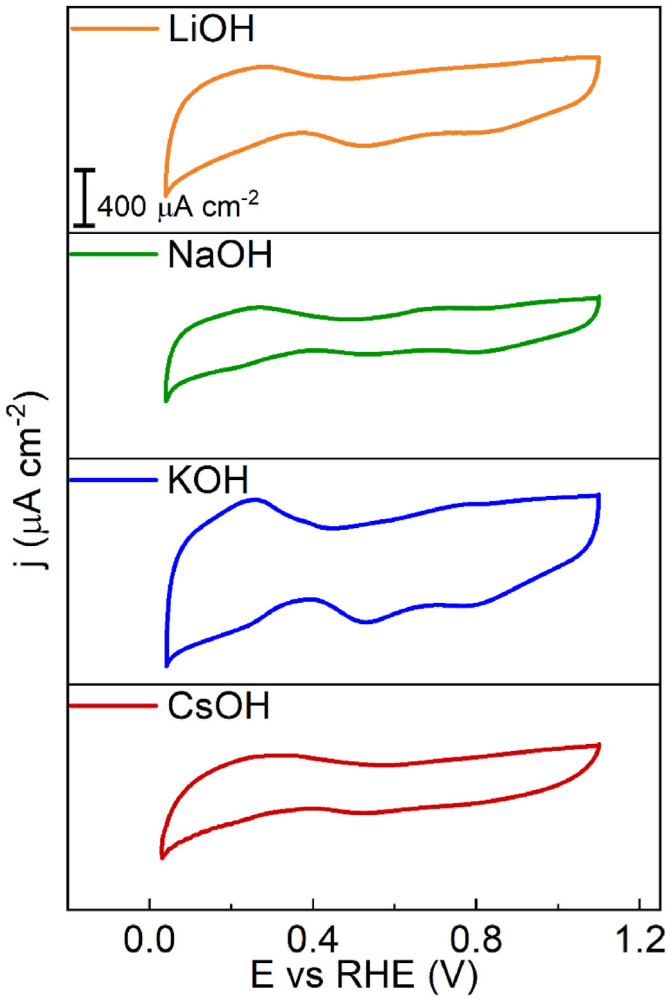

Fig. 2. Typical cyclic voltammograms of Pt-microelectrodes obtained at the scan rate of 50 mV s^{-1} in Ar-saturated 0.1 M AMOH electrolytes (AM = Li^+, Na^+, K^+, Cs^+).

employed to evaluate the HER thermodynamics. The HER was analyzed using clean metal surfaces to simplify our model. The free energies for all systems were computed, including zero-point energy (ZPE) and vibrational entropy S_{vib} contributions taken at 300 K as $\Delta G = E_{DFT} + ZPE - TS_{vib}$. All other computational details and supporting data are provided in the supporting information (SI).

3. Results and discussion

Fig. 1 shows the HER activity data for the polycrystalline Pt (Pt(pc)) disc electrodes measured in the H_2 saturated 0.1 M AMOH (AM = Li^+, Na^+, K^+, Cs^+) electrolytes at low overpotentials. Curves recorded in different electrolytes are very similar in shape but shifted. The Tafel slopes vary only slightly (between ca 79 and ca 93 $mVdec^{-1}$), indicating that the RDS is the same in all cases. Nevertheless, the exchange current density was observed to decrease in the following order: LiOH ≥ NaOH > KOH > CsOH, from ca 0.84 to ca 0.21 mA cm^{-2} (Fig. 1). These cation-dependent phenomena indicate a change in the interfacial water structure and the binding energy of adsorbed hydrogen species caused by the high concentration of cations on the Pt surface [4,11]. Considering that the Tafel slope (Fig. 1) is not constant till −0.05 V, it is of particular interest to use EIS and elucidate the contribution of each mechanism in this potential region. For this purpose, Pt microelectrodes with a diameter of 25 μm were used. The application of the microelectrode allows for suppressing mass transfer limitations and ohmic drop issues due to its small dimension, which is undesirable for kinetics measurements.

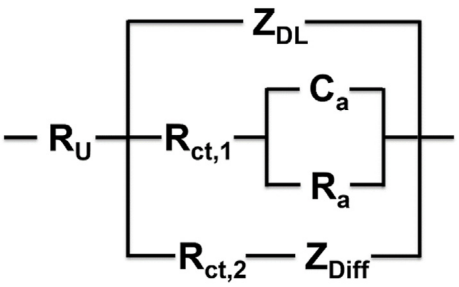

Fig. 3. The equivalent electric circuit describing the impedance response of the Pt-microelectrodes in H_2-saturated 0.1 M AMOH electrolytes (AM = Li^+, Na^+, K^+, Cs^+).

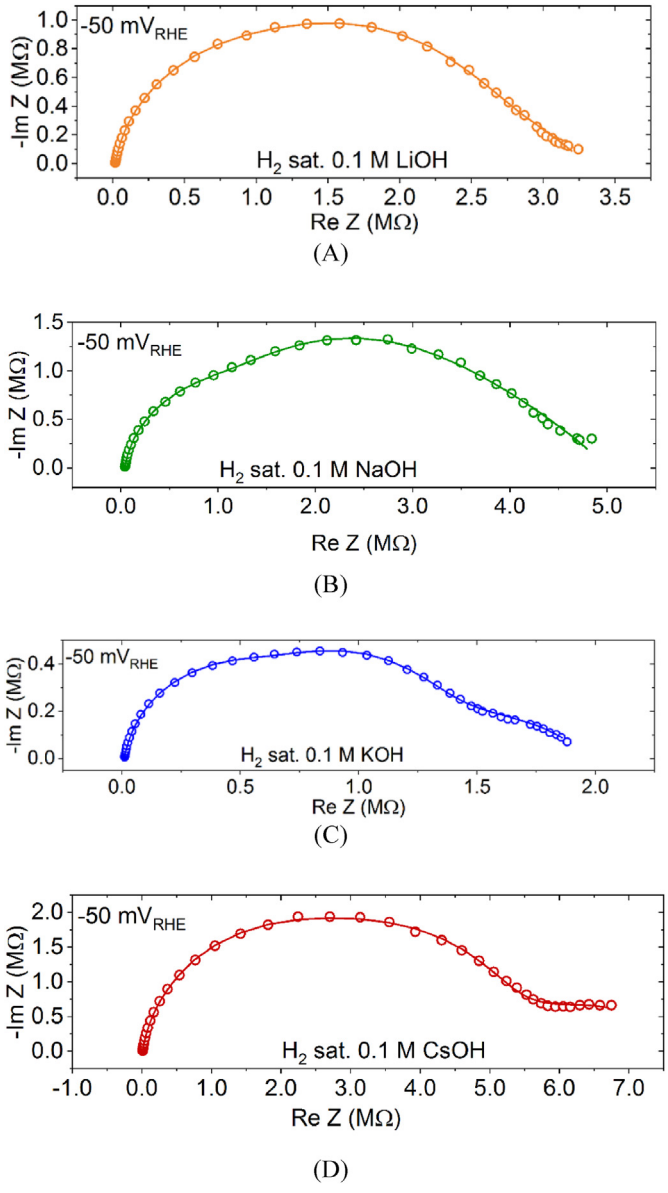

Fig. 4. Typical examples of fitting of the EIS data to the model shown in Fig. 3 for the: (A) LiOH, (B) NaOH, (C) KOH, and (D) CsOH at −0.05 V vs RHE. Solid lines represent the fitting, while the points represent the raw data.

Typical cyclic voltammograms of Pt-microelectrodes recorded in the Ar-saturated 0.1 M LiOH, NaOH, KOH, and CsOH electrolytes are shown

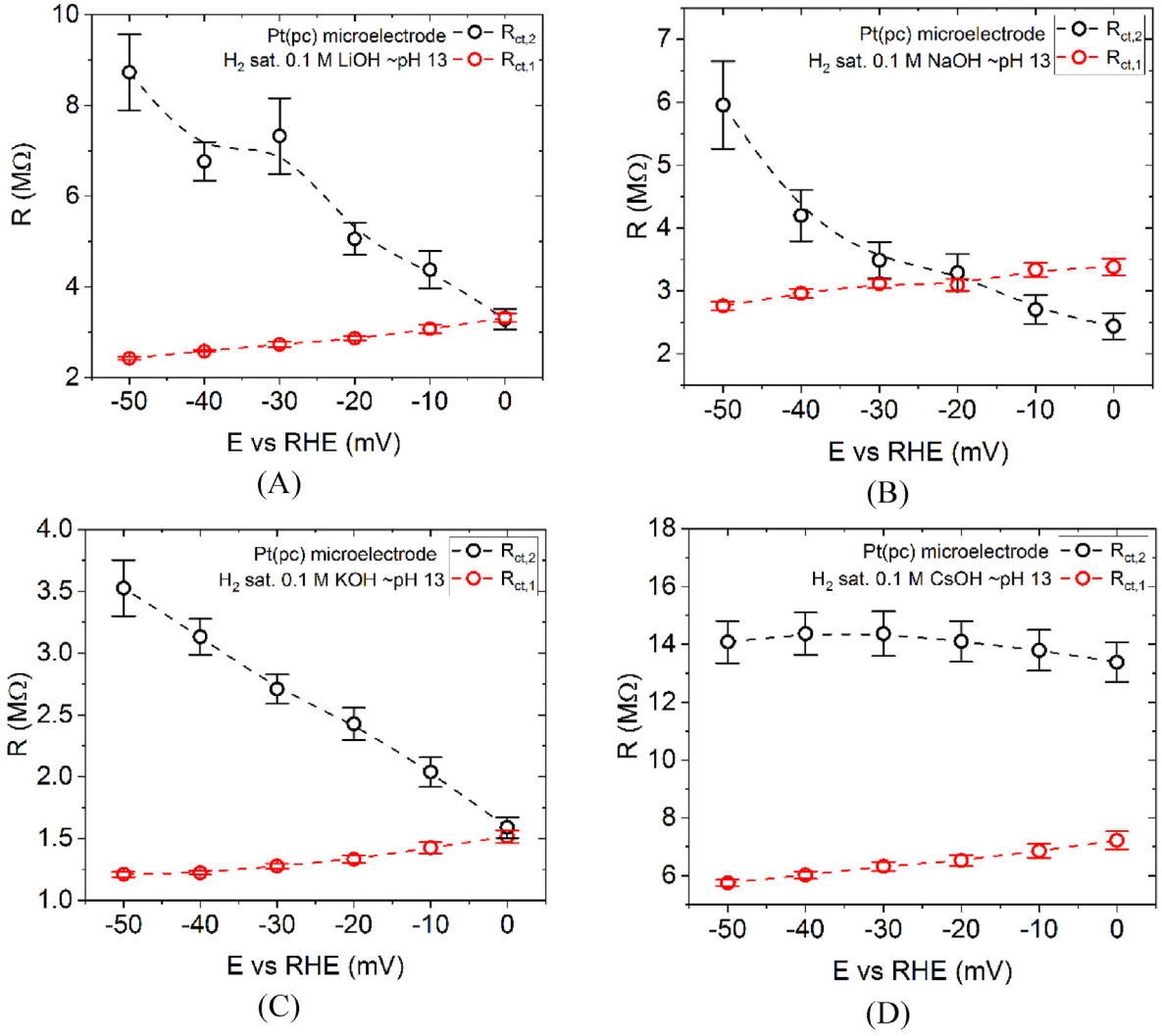

Fig. 5. Charge transfer resistances associated with the VH, $R_{ct,1}$, and VT, $R_{ct,2}$, mechanisms for (A) 0.1 M LiOH, (B) 0.1 M NaOH, (C) 0.1 M KOH and (D) 0.1 M CsOH electrolytes at low overpotentials.

in Fig. 2. Shapes of the voltammograms in the hydrogen adsorption/desorption regions are clearly different in the presence of various AM cations. As adsorbed hydrogen species are also intermediates in the HER, AM cations likely affect the surface's adsorption properties during the hydrogen evolution.

We assume in our impedance analysis that the physical model developed in our previous work [20] for the HER in acidic media is also valid at higher pH values (Fig. 3). The model consists of the uncompensated resistance, R_U, the impedance of the double layer, Z_{DL}, and two parallel branches consisting of elements associated with the VH and VT pathways. The charge transfer resistance, $R_{ct,1}$, adsorption pseudocapacitance, C_a, and adsorption resistance, R_a, are associated with the Heyrovsky mechanism. Consequently, the VT pathway manifests itself by two elements, the charge transfer resistance, $R_{ct,2}$, and the semi-infinite linear diffusional Warburg impedance, Z_{Diff}. For the derivation of the model and detailed explanation, we refer to Ref. [20].

The ratio of the charge transfer resistances, $R_{ct,2}/R_{ct,1}$, provides an estimate for the relative contribution of the VH and VT mechanisms to the total measured current in the absence of significant diffusion limitations [20].

Fig. 4 shows that the model described in Fig. 3 can provide good fitting results with relatively small root-mean-squared deviations for all electrolyte compositions investigated in this work. Estimated individual parameter uncertainties confirm that each element contributes to the

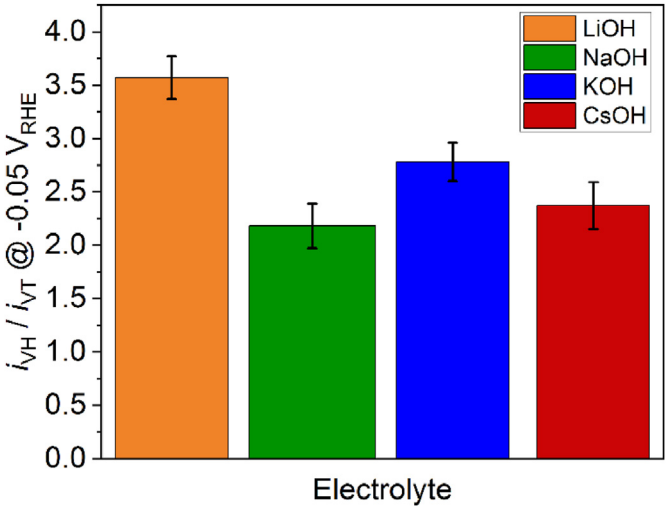

Fig. 6. The relative contribution of the currents for the VH and VT mechanisms for 0.1 M LiOH, NaOH, KOH, and CsOH electrolytes at −0.05 V vs. RHE on Pt-microelectrodes. As one can see, the VH mechanism dominates more profoundly in the LiOH electrolyte.

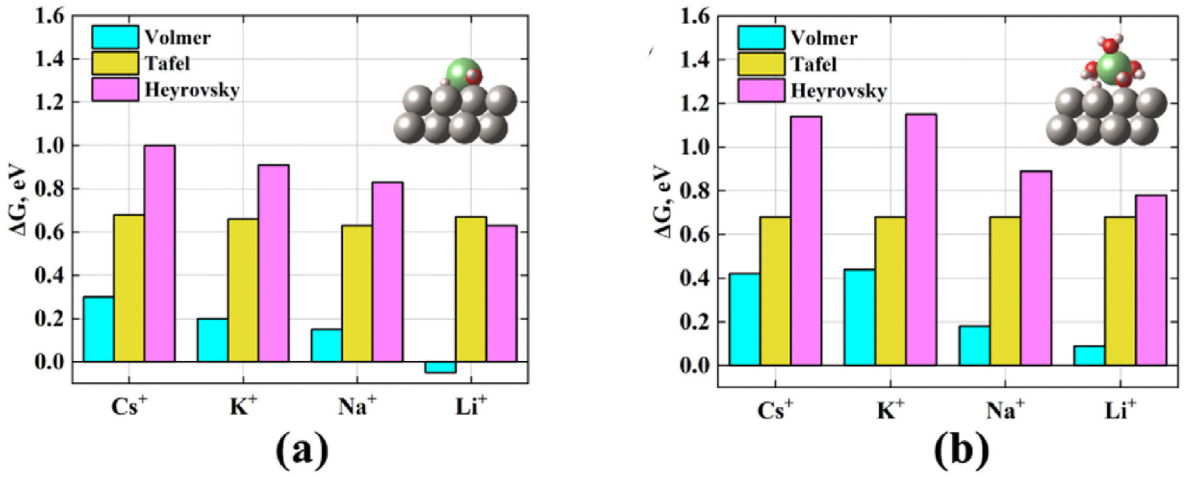

Fig. 7. Reaction free energies computed for the Volmer, Tafel, and Heyrovsky steps of the HER on the pristine Pt(111) surface and in the presence of alkali metal cations. The results for bare and solvated cations are presented on the left (a) and right (b) side, respectively, with the exemplary atomic-structure snapshots for the Li^+ case. Only the most energetically favorable reaction pathways found for each step (see Figure S7) are shown for clarity, while all the data are provided in Section "Details on the DFT calculations" of SI.

overall description of the EIS response (see Figures S1-S4 and Tables S1-S4 in the SI).

Fig. 5 illustrates that the relative contribution of the VH and VT steps differs for the explored cations and changes with the overpotential. The contribution of the VH mechanism dominates with increasing overpotential for all investigated electrolytes. Remarkably, the HER mechanism depends on the overpotential for 0.1 M NaOH (Fig. 5B) with the major contribution of VT being observed at lower overpotentials and VH being the dominating mechanism at higher overpotentials. In 0.1 M CsOH, VH is the dominating mechanism independent of the applied overpotential (Fig. 5D). The ratio $R_{ct,2}/R_{ct,1} = i_{VH}/i_{VT}$, where i_{VH} and i_{VT} are the partial currents due to the VH and VT mechanisms, respectively, gives the relative contribution of the VT and VH mechanisms to the observed current (Fig. 6). As shown in Fig. 6, the VH mechanism dominates in the presence of Li^+ at higher overpotentials.

DFT simulations are employed to analyze the role of AM on the HER mechanism for the reference Pt(111) surface by evaluating the binding energies of *H and *OH (HBE and OHBE, respectively). Our calculations reveal that HBE is almost unaffected by the presence of the cations on the surface. This is, however, different in the case of OH-adsorption as a significant effect of the cations on the energetics of OH-adsorption and water dissociation is determined (see Tables S6 and S10 in the SI). Figure S6 shows a clear correlation between OHBE and the hydration energy of the corresponding AM cation revealing the strongest driving force for OH-binding to the Pt surface with Li^+. This is because alkali metal cations energetically prefer to form direct chemical bonds with the adsorbed OH species. Specifically, in addition to considering bare cations at the surfaces, we include cations with their first water shell in the analysis. In this case, we find that the outer-sphere aqueous cation complexes always converge to more stable inner-sphere complexes with direct M − OH bonds at the interface during DFT optimization calculations. The stability of such complexes at the metal surfaces is confirmed by additional AIMD simulations at room temperature (see SI for further details).

Next, we proceed with investigating the HER pathways for the Pt(111) surface in the presence of AM cations. Although the presence of adsorbed H-species is necessary for the reaction to proceed *via* either the Tafel or Heyrovsky step, in practice, different reaction pathways at the interface are conceivable. We systematically examine various reaction scenarios that are schematically displayed in Figure S7. Specifically for the Volmer step, we can identify three different reaction pathways: 1) H^+ is adsorbed on the surface, while OH^- goes to the solution (denoted as V1 in Figure S7), 2) both H^+ and OH^- are adsorbed on the surface (V2), and 3) OH^- is adsorbed, while H^+ goes to the solution (V3). The Heyrovsky step can be analogously classified, resulting in five possibilities denoted as the H1–H5 pathways in Figure S7.

Fig. 7 shows the results for the most energetically favorable pathways of the HER over Pt(111) identified in our calculations. It can be seen that AM cations systematically decrease the energetics of the Volmer and Heyrovsky reaction steps in the sequence $Cs^+ < K^+ < Na^+ < Li^+$, while the Tafel step remains almost unaffected. It is also seen from Fig. 7b that the cation trend is preserved when the first aqueous shell is included in calculations. Overall, our computational results appear to agree with the electrochemical measurements discussed above. Specifically, simulations demonstrate that AM cations should change the relative contribution of the VT and VH mechanisms to the overall HER process, with Li^+ promoting the VH mechanism more than other cations.

The Bader charge analysis agrees well with the computed HER thermodynamics. Figure S5 shows the computed Bader charges on Pt centers directly underneath the OH adsorbates. It can be seen that the atomic charges systematically decrease when going from the pure metal cases to the Li^+ system. As expected from the HER energetics, the weakest effect is observed for Cs^+ and the strongest one for Li^+.

4. Conclusions

The found enhancement of the HER activity on Pt electrodes at 0.1 M concentration of AM cations follows the trend: $Li^+ \geq Na^+ > K^+ > Cs^+$, where the highest activity results from LiOH electrolytes at low overpotentials. We show that the nature of AM cations and overpotential can influence the contribution of VH and VT mechanisms in the HER. The presence of Li^+ ions, in general, promotes the VH mechanism at the overpotential close to −0.05 V vs RHE. Experimental results are supported by DFT calculations revealing that the Volmer and Heyrovsky reaction steps become more favorable when progressing from Cs^+ to Li^+, while the Tafel step is not sensitive to the nature of AM. In summary, the presence of "spectator" AM cations impacts the reaction energetics and allows steering the process along a specific reaction pathway.

Declaration of competing interest

The authors declare that they have no known competing financial interests or personal relationships that could have appeared to influence the work reported in this paper.

Acknowledgments

We want to thank the German Research Foundation (DFG) under Germany's excellence strategy – EXC 2089/1 – 390776260, Germany's excellence cluster "e-conversion", and the DFG project BA 5795/6-1. This project has received additional funding from the European Union's Horizon 2020 research and innovation program under grant agreement HERMES No 952184. VA acknowledges the National Science Foundation (NSF) support through the NSF CAREER award (Grant No. CBET-1941204). ASB acknowledges financial support from TUM Innovation Network for Artificial Intelligence powered Multifunctional Material Design (ARTEMIS). We also acknowledge the Leibniz Supercomputing Centre at TUM for providing computational support.

Appendix A. Supplementary data

Supplementary data to this article can be found online at https://doi.org/10.1016/j.nanoms.2022.09.003.

References

[1] Y. Zheng, Y. Jiao, A. Vasileff, S.-Z. Qiao, Angew. Chem. Int. Ed. (2018), https://doi.org/10.1002/anie.201710556.
[2] I. Ledezma-Yanez, W.D.Z. Wallace, P. Sebastián-Pascual, V. Climent, J.M. Feliu, M.T.M. Koper, Nat. Energy (2017), https://doi.org/10.1038/nenergy.2017.31.
[3] B. Deng, M. Huang, X. Zhao, S. Mou, F. Dong, ACS Catal. (2021), https://doi.org/10.1021/acscatal.1c03501.
[4] B. Huang, R.R. Rao, S. You, K.H. Myint, Y. Song, Y. Wang, W. Ding, L. Giordano, Y. Zhang, T. Wang, S. Muy, Y. Katayama, J.C. Grossman, A.P. Willard, K. Xu, Y. Jiang, Y. Shao-Horn, JACS Au (2021), https://doi.org/10.1021/jacsau.1c00281.
[5] X. Ding, D. Scieszka, S. Watzele, S. Xue, B. Garlyyev, R.W. Haid, A.S. Bandarenka, Chemelectrochem (2022), https://doi.org/10.1002/celc.202101088.
[6] J. Li, J.H. Stenlid, T. Ludwig, P.S. Lamoureux, F. Abild-Pedersen, JACS (2021), https://doi.org/10.1021/jacs.1c07276.
[7] R. Subbaraman, D. Tripkovic, D. Strmcnik, K.-C. Chang, M. Uchimura, A.P. Paulikas, V. Stamenkovic, N.M. Markovic, Science (2011), https://doi.org/10.1126/science.1211934.
[8] B. Garlyyev, S. Xue, S. Watzele, D. Scieszka, A.S. Bandarenka, J. Phys. Chem. Lett. (2018), https://doi.org/10.1021/acs.jpclett.8b00610.
[9] S. Xue, B. Garlyyev, A. Auer, J. Kunze-Liebhäuser, A.S. Bandarenka, J. Phys. Chem. C (2020), https://doi.org/10.1021/acs.jpcc.0c01715.
[10] R.W. Haid, X. Ding, T.K. Sarpey, A.S. Bandarenka, B. Garlyyev, Curr. Opin. Electrochem. (2022), https://doi.org/10.1016/j.coelec.2021.100882.
[11] S. Xue, B. Garlyyev, S. Watzele, Y. Liang, J. Fichtner, M.D. Pohl, A.S. Bandarenka, Chemelectrochem (2018), https://doi.org/10.1002/celc.201800690.
[12] W. Sheng, Z. Zhuang, M. Gao, J. Zheng, J.G. Chen, Y. Yan, Nat. Commun. (2015), https://doi.org/10.1038/ncomms6848.
[13] R. Subbaraman, D. Tripkovic, K.C. Chang, D. Strmcnik, A.P. Paulikas, P. Hirunsit, M. Chan, J. Greeley, V. Stamenkovic, N.M. Markovic, Nat. Mater. (2012), https://doi.org/10.1038/NMAT3313.
[14] W. Ni, T. Wang, F. Héroguel, A. Krammer, S. Lee, L. Yao, A. Schüler, J.S. Luterbacher, Y. Yan, X. Hu, Nat. Mater. (2022), https://doi.org/10.1038/s41563-022-01221-5.
[15] E. Liu, J. Li, L. Jiao, H.T.T. Doan, Z. Liu, Z. Zhao, Y. Huang, K.M. Abraham, S. Mukerjee, Q. Jia, J. Am. Chem. Soc. (2019), https://doi.org/10.1021/jacs.8b13228.
[16] D. Strmcnik, K. Kodama, D. Van der Vliet, J. Greeley, V.R. Stamenkovic, N.M. Marković, Nat. Chem. (2009), https://doi.org/10.1038/nchem.330.
[17] B. Garlyyev, S. Xue, M.D. Pohl, D. Reinisch, A.S. Bandarenka, ACS Omega (2018), https://doi.org/10.1021/acsomega.8b00298.
[18] A. Goyal, M.T.M. Koper, Angew. Chem. Int. Ed. (2021), https://doi.org/10.1002/anie.202102803.
[19] X. Chen, I.T. McCrum, K.A. Schwarz, M.J. Janik, M.T.M. Koper, Angew. Chem. Int. Ed (2017), https://doi.org/10.1002/anie.201709455.
[20] S. Watzele, J. Fichtner, B. Garlyyev, J.N. Schwämmlein, A.S. Bandarenka, ACS Catal. (2018), https://doi.org/10.1021/acscatal.8b03365.
[21] H.T. Chung, U. Martinez, I. Matanovic, Y.S. Kim, J. Phys. Chem. Lett. (2016), https://doi.org/10.1021/acs.jpclett.6b02025.
[22] J. Durst, C. Simon, A. Siebel, P.J. Rheinländer, T. Schuler, M. Hanzlik, J. Herranz, F. Hasché, H.A. Gasteiger, ECS Trans. (2014), https://doi.org/10.1149/06403.1069ecst.
[23] S. Watzele, Y. Liang, A.S. Bandarenka, ACS Appl. Energy Mater. (2018), https://doi.org/10.1021/ACSAEM.8B00852.
[24] A.S. Bondarenko, Anal. Chim. Acta (2012), https://doi.org/10.1016/j.aca.2012.06.055.
[25] A.S. Bandarenka, Development of hybrid algorithms for EIS data fitting, a book chapter in, in: O. Kanoun (Ed.), Lecture Notes on Impedance Spectroscopy. Measurement, Modeling and Applications vol. 4, CRC Press, Tailor and Francis Group, London, 2013, ISBN 9780429227578, pp. 29–36.
[26] J.P. Perdew, K. Burke, M. Ernzerhof, Phys. Rev. Lett. (1997), https://doi.org/10.1103/PhysRevLett.78.1396.
[27] Y. Zhang, W. Yang, Phys. Rev. Lett. (1998), https://doi.org/10.1103/PhysRevLett.80.890.
[28] G. Kresse, J. Furthmüller, Phys. Rev. B (1996), https://doi.org/10.1103/PhysRevB.54.11169.
[29] G. Kresse, J. Furthmüller, Comput. Mater. Sci. (1996), https://doi.org/10.1016/0927-0256(96)00008-0.
[30] S. Grimme, J. Antony, S. Ehrlich, H. Krieg, J. Chem. Phys. (2010), https://doi.org/10.1063/1.3382344.
[31] S. Grimme, S. Ehrlich, L. Goerigk, J. Comput. Chem. (2011), https://doi.org/10.1002/jcc.21759.
[32] K. Momma, F. Izumi, J. Appl. Crystallogr. (2011), https://doi.org/10.1107/S0021889811038970.
[33] T. Cheng, L. Wang, B.V. Merinov, W.A. Goddard III, J. Am. Chem. Soc. (2018), https://doi.org/10.1021/jacs.8b04006.
[34] A. Bouzid, P. Gono, A. Pasquarello, J. Catal. (2019), https://doi.org/10.48550/arXiv.1912.07269.
[35] I.T. McCrum, M.J. Janik, J. Phys. Chem. C (2016), https://doi.org/10.1021/acs.jpcc.5b10979.
[36] J.N. Mills, I.T. McCrum, M.J. Janik, Phys. Chem. Chem. Phys. (2014), https://doi.org/10.1039/C4CP00760C.
[37] I.C. Man, H.-Y. Su, F. Calle-Vallejo, H.A. Hansen, J.I. Martínez, N.G. Inoglu, J. Kitchin, T.F. Jaramillo, J.K. Nørskov, J. Rossmeisl, ChemCatChem (2011), https://doi.org/10.1002/cctc.201000397.
[38] J.K. Nørskov, J. Rossmeisl, A. Logadottir, L. Lindqvist, J.R. Kitchin, T. Bligaard, H. Jonsson, J. Phys. Chem. B (2004), https://doi.org/10.1021/jp047349j.